Dyes and Pigments 136 (2017) 31–45

Contents lists available at ScienceDirect

Dyes and Pigments

journal homepage: www.elsevier.com/locate/dyepig

Novel pyrazino-phenanthroline based rigid donor-π-acceptor compounds: A detail study of optical properties, acidochromism, solvatochromism and structure-property relationship

Shantaram Kothavale, Nagaiyan Sekar*

Department of Dyestuff Technology, Institute of Chemical Technology, Matunga, Mumbai, 400 019, India

ARTICLE INFO

Article history:
Received 28 May 2016
Received in revised form
12 August 2016
Accepted 13 August 2016
Available online 15 August 2016

Keywords:
Fused ring pyrazine
Acidochromism
Solvatochromism
Structure-property relationship
Multi-linear regression analysis
Density function theory

ABSTRACT

Donor-π-acceptor-π-auxiliary acceptor type compounds have been designed and synthesized to study their rigidity and structural effects on optical properties. Structural variation is achieved by changing the central π-conjugated core with naphthalene, acenaphthene and phenanthrene based donor-π-acceptor compounds containing *N*, *N*-diethyl aniline or morpholine as donor and pyrazine ring fused with phenanthroline as acceptor. A detailed study of positive and negative acidochromism is performed. Intramolecular charge transfer, solvatochromism and highly polar excited state of these compounds are elucidated by Lippert-Mataga, Mac-Rae and Reichardt correlations. Multilinear regression analysis using Kamlet-Taft and Catalan parameters is also performed to support the observed solvatochromism in absorption and emission spectra from non-polar to polar solvents. All the spectroscopic results were correlated theoretically by Density Functional Theory (DFT) computations.

© 2016 Elsevier Ltd. All rights reserved.

1. Introduction

Rigid polyaromatic planar heterocyclic compounds with donor-π-acceptor architecture have attracted much attention in recent years due to their special electro-optical properties originating from their low band gap [1,2]. Due to their facile synthesis, versatility, strong electron-withdrawing ability and easy functionalization different pyrazine derivatives such as 2, 3-diphenylquinoxaline [3–6], thienopyrazine [7–9], pyridopyrazine [10,11] have been successfully implemented in field effect transistors [12–14], photovoltaic devices [15,16] and light-emitting diodes (LEDs) [17–20]. At the same time, several researchers have developed pyrazine or quinoxaline based organic sensitizers for their high performance in dye sensitized solar cells (DSSC) [21–25]. Different pyrazine mediated π-extended long chain fused azacene derivatives have been reported [26,27] and applied in bulk heterojunction organic solar cells [28,29], n-type organic semiconductors [30–33] and as charge transfer species [34–38].

Dipyrido[3,2-a:2′,3’-c]phenazine (dppz) ligand is a combination of 1, 10 phenanthroline and quinoxaline system. The diimine site of dppz allows coordination with various transition metal ions to yield stable metal–organic complexes and introduction of functional groups in the dppz core can fine tune the HOMO-LUMO gaps of resultant compounds [39–42]. As the pyrazine core in dppz ligand acts as an electron acceptor, its intramolecular charge transfer (ICT) character was tested by attaching different electron donating group on the side arms at different positions keeping two more nitrogen free as the metal chelating site [43,44]. Novel fused pyrazino-phenanthroline systems with ICT and solvent sensitive emission behavior were studied also [45].

A very good structure-property relationship, variation in band gap and strengthening of ICT character was found after fusing thiophene or benzene rings and/or putting additional donating groups on main pyrazine core at different locations [36,46–48]. The environment sensitive fluorescent dyes e.g. solvatochromic dyes, found their applications for monitoring protein, DNA and bio-membranes. These dyes show strong changes in their dipole moments upon electronic excitation and thus show red shift in their emission maximum upon an increase in polarity of the solvent environment [49–53]. Few phenazine based solvatochromic dyes are also reported where pyrazine core acts as electron acceptor [54–56]. Recently from our group phenazine fused benzocoumarins were reported where negative and positive solvatochromisms

---

* Corresponding author.
E-mail addresses: n.sekar@ictmumbai.edu.in, nethi.sekar@gmail.com (N. Sekar).

http://dx.doi.org/10.1016/j.dyepig.2016.08.032
0143-7208/© 2016 Elsevier Ltd. All rights reserved.

were observed [57,58].

On protonation of the central electron withdrawing nitrogen of different pyridine type heterocyclic compounds enhancement in electron withdrawing ability and stabilization of LUMO were observed causing a dramatic red-shift in absorption [59–62]. Few nitrogen containing heterocycles were also studied for their acidochromic properties where extraordinary red shift in absorption λmax was observed on addition of TFA [63–66].

We synthesized four novel benzo*[h]*dipyrido[3,2-a:2′,3'-c]phenazine derivatives where 5,6-diaminophenanthroline was used to obtain more more extended conjugation with two more free nitrogen atoms as metal chelating sites and as supporting electron acceptor. To get the desired amine substituted phenazine derivatives we used potassium 3,4-dioxo-3,4-dihydronaphthalene-1-sulfonate instead of naphthalene-1,2-dione which was synthesized by following the reported procedure [67] where the sulfonate salt acts as better leaving group than hydrogen in a Michael type addition. We synthesized two more derivatives by substituting 5-bromoacenaphthylene-1, 2-dione and 3-bromophenanthrene-9, 10-dione with morpholine to study the structural effects on the electrochemical and photophysical properties. The respective 5-bromoacenaphthylene-1, 2-dione and 3-bromophenanthrene-9, 10-dione intermediates were synthesized by following the reported procedure [68,69]. As the donor-acceptor interaction in such molecules is mainly dependent on the strength of the donor or acceptor, conjugation length and nature of the conjugating unit, we incorporated almost same donating group i.e. morpholine and varied the conjugation length except in the case of compound **4** where N, *N*-diethyl aniline was used as donating group. The structures of all the four newly synthesized donor-acceptor compounds are represented in Fig. 1.

2. Experimental section

2.1. Materials and equipments

All the required chemicals were obtained from commercial sources and used as received without any further purification. The solvents used for synthesis and analytical measurements were obtained from S. D. Fine Chemicals (India), dried by following standard procedures and distilled prior to use. All the reactions were monitored by TLC (thin layer chromatography) with detection by UV light. 100–200 Mesh silica was used in column chromatography as the stationary phase for purification. ^{1}H and ^{13}C NMR spectral data were recorded on a 500 MHz instrument using TMS as an internal standard. Mass spectra were recorded on Finnigen mass spectrometer and HRMS analysis was done using a QTOF LC/MS spectrometer. The absorption and emission spectra were recorded at room temperature using a 10 mm cuvette with a 2.5 nm slit width. Emission quantum yields were obtained by using coumarin-6 (ΦF = 0.94 in chloroform) as reference. Cyclic voltammetry experiments were performed using glassy carbon (2 mm diameter) as working electrode, platinum wire as counter electrode, and standard calomel electrode as reference electrode with 0.1 M solution of tetrabutylammonium hexafluorophosphate (TBu_4NPF_6) as supporting electrolyte in DCM solvent.

2.2. Computational methods

The ground state (S_0) geometry of all compounds was optimized using Density Functional Theory (DFT) [70] by using the Gaussian 09 package and the popular hybrid functional B3LYP. The B3LYP combines Becke's three parameter exchange functional (B3) [71] with the nonlocal correlation functional by Lee, Yang, and Parr (LYP) [72]. The basis set used for all atoms was 6-31G (d) in both DFT and time-dependent density functional theory (TD-DFT) method. The low-lying first singlet excited states (S1) of the dyes were relaxed to obtain their minimum energy geometries using the TD-DFT. The vertical excitation energies and oscillator strengths were obtained for the lowest 10 singlet-singlet transitions at the optimized ground state equilibrium geometries by using TD-DFT at the same hybrid functional and basis set [73]. Emissions were obtained by calculating difference between the energies of the optimized geometries at first singlet excited state and ground state. Frequency computations were also carried out on the optimized geometry of the low-lying vibronically relaxed first excited state of conformers. The computations in various solvent media were carried out using the self-consistent reaction field (SCRF) under the polarizable continuum model (PCM) [74]. Optimized ground structures were utilized to obtain the electronic absorption spectra, including maximum absorption and emission wavelengths, oscillator strengths, and main configuration assignment by using TD-DFT with the PCM model.

2.3. Synthesis

2.3.1. synthesis of 4-(4-(diethylamino)phenyl)naphthalene-1,2-dione (2)

The diketo compound (2.8 g, 10.13 mmol) was dissolved in methanol: water (3:1) (30 mL) and then *N,N* diethyl aniline (2.1 mL, 13.173 mmol) was added in the reaction mixture slowly and stirred for 24 h at room temperature. On completion the reaction mixture was concentrated by evaporating methanol. The dark blue colored solid separated out was filtered and dried well to get pure product

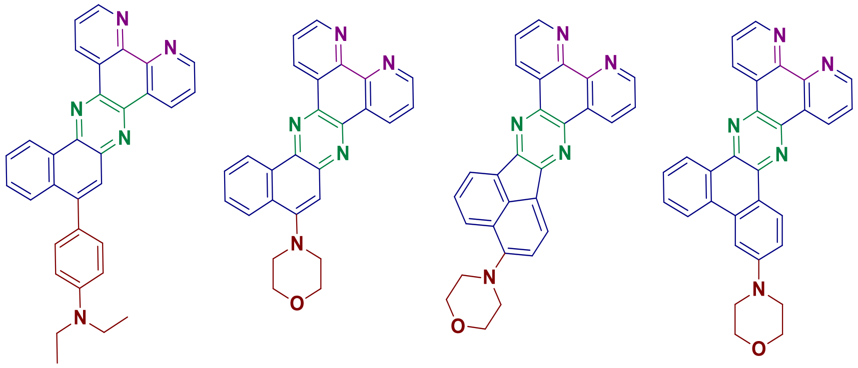

4 **5** **9** **13**

Fig. 1. Structure of the synthesized compounds.

(1.4 g). The filtrate was further concentrated to its half amount and filtered again to get the second crop of the product (0.4 g). Yield = 1.8 g (58.25%). Melting point = 128–133 °C. ^{1}H NMR (500 MHz, CDCl$_3$): δ 1.22–1.24 (t, J = 5.5, 6H), 3.43–3.45 (q, 4H), 6.43 (s, 1H), 6.73–6.75 (d, J = 7.5, 2H), 7.36–7.38 (d, J = 7.5, 2H), 7.51–7.59 (m, 3H), 8.16–8.18 (d, J = 6.5, 1H). ^{13}C NMR (125 MHz, CDCl$_3$): δ 12.57, 44.51, 111.03, 122.54, 125.46, 129.86, 130.28, 130.32, 130.41, 132.00, 134.64, 135.35, 149.29, 157.44, 180.19, 180.52.

2.3.2. synthesis of 4-morpholinonaphthalene-1,2-dione (3)

The diketo compound (2.8 g, 10.13 mmol) was dissolved in minimum amount of water and then morpholine (2.1 mL, 13.173 mmol) was added slowly. Red colored product separated out immediately. After stirring for 10 min the reaction mixture was cooled to 0 °C, filtered and dried to get the pure product (1.8 g, 58.25%). Melting point = 164–168 °C. ^{1}H NMR (500 MHz, CDCl$_3$): δ 3.35–3.37 (t, J = 4.5, 4H), 3.92–3.94 (t, J = 5, 4H), 5.98 (s, 1H), 7.52–7.57 (m, 2H), 7.63–7.66 (t, J = 7.5, 1H), 8.09–8.11 (d, J = 7.5, 1H). ^{13}C NMR (125 MHz, CDCl$_3$): 51.63, 66.21, 109.84, 126.70, 129.80, 130.93, 132.02, 132.06, 134.23, 163.39, 178.71, 180.34.

2.3.3. synthesis of 5-morpholinoacenaphthylene-1,2-dione (8)

Compound **7** (1 g, 3.831 mmol) was dissolved in N, N dimethyl acetamide (10 mL), K$_2$CO$_3$ (0.79 g, 5.747 mmol) and CuI (0.72 g, 3.831 mmol) followed by morpholine (0.49 mL, 5.747 mmol) was added and the mixture was heated at 90 °C for 4 h. Water was added to the red colored reaction mixture at room temperature. The solid precipitated out was filtered, dried and purified by column chromatography using 20% EtOAc in hexane to get the pure product. (0.61 g, 59.80%) Melting point = 222–227 °C. ^{1}H NMR (500 MHz, CDCl$_3$): δ 3.38–3.40 (t, J = 4.5, 4H), 4.02–4.04 (t, J = 4.5, 4H), 7.20–7.21 (d, J = 8, 1H), 7.72–7.75 (t, J = 7.5, 1H), 7.99–8.00 (d, J = 7, 1H), 8.04–8.05 (d, J = 8, 1H), 8.23–8.25 (d, J = 8.5, 1H). ^{13}C NMR (125 MHz, CDCl$_3$): δ 52.51, 66.84, 115.13, 121.92, 123.43, 124.05, 124.83, 127.08, 128.88, 129.49, 148, 154.68, 186.24, 189.51.

2.3.4. synthesis of 3-morpholinophenanthrene-9,10-dione (12)

Compound **11** (1 g, 3.483 mmol), K$_2$CO$_3$ (0.72 g, 5.224 mmol), CuI (0.13 g, 0.696 mmol) were dissolved in DMF (10 mL). Morpholine (0.45 g, 5.224 mmol) was slowly added and the mixture was heated at 90 °C for 4 h. After completion water was added to the reaction mixture and extracted with ethyl acetate (3 × 50 mL). The organic layer was evaporated on rotavapour after passing through anhydrous Na$_2$SO$_4$ and the crude product obtained was purified on column chromatography (15% EtOAc in hexane) to get the pure product (0.47 g, 46.07%). Melting point = 252–256 °C. ^{1}H NMR (500 MHz, CDCl$_3$): δ 3.54–3.56 (t, J = 5, 4H), 3.73–3.75 (t, J = 5.5, 4H), 7.00–7.05 (dd, J = 9 and 2.5, 1H), 7.49–7.53 (t, J = 8, 1H), 7.59–7.60 (d, J = 2.5, 1H), 7.73–7.76 (td, J = 7.5 and 1.5, 1H), 7.87–7.89 (d, J = 9, 1H), 7.96–7.98 (dd, J = 8 and 1.5, 1H), 8.40–8.41 (d, J = 7.5, 1H). ^{13}C NMR (125 MHz, CDCl$_3$): δ 51.97, 71.28, 113.10, 119.04, 126.62, 130.20, 134.20, 134.85, 136.74, 137.68, 140.65, 141.05, 142.46, 160.96, 181.91, 186.20.

2.3.5. General procedure for the synthesis of compound 4, 5, 9, 13

The respective diketo compound and 1, 10-phenanthroline-5, 6-diamine were dissolved in methanol followed by catalytic amount of acetic acid and the mixture was refluxed for 5–6 h. The mixture was cooled to room temperature and the solid separated was filtered, washed with small amount of cold methanol followed by hexane and dried well to get red colored product.

2.3.5.1. 4-(Benzo[h]dipyrido[3,2-a:2′,3′-c]phenazin-14-yl)-N,N-diethylaniline (4). Compound **4** was synthesized by following the general procedure described above. 1, 10-Phenanthroline-5, 6-diamine (0.4 g, 1.902 mmol) and compound 2 (0.75 g, 2.473 mmol) were refluxed in methanol. (Yield: 0.75 g, 82.23%). Melting point = 256 °C. ^{1}H NMR (500 MHz, CDCl$_3$): δ 1.22–1.24 (t, J = 5.5, 6H), 3.43–3.45 (q, 4H), 6.43 (s, 1H), 6.73–6.75 (d, J = 7.5, 2H), 7.26–7.59 (m, 6H), 8.16–8.18 (d, J = 6.5, 1H). ^{13}C NMR (125 MHz, CDCl$_3$): δ 12.37, 29.66, 123.81, 125.26, 127.00, 127.32, 127.47, 127.61, 129.26, 131.10, 133.30, 140.28, 140.54, 142.21, 147.65, 147.73, 151.86, 152.00. HRMS (ESI): *m*/*z* calcd for $(M + H)^+$ $C_{32}H_{25}N_5$ 480.2182; found 480.2158.

2.3.5.2. 4-(Benzo[h]dipyrido[3,2-a:2′,3′-c]phenazin-14-yl)morpholine (5). Compound **5** was synthesized by following the general procedure described above 1, 10-phenanthroline-5, 6-diamine (0.3 g, 1.427 mmol) and compound **3** (0.45 g, 1.855 mmol) refluxed in methanol. (Yield: 0.5 g, 84.03%). Melting point = 282 °C. ^{1}H NMR (500 MHz, CDCl$_3$): δ 3.32–3.33(3, 4H), 4.07–4.08 (t, J = 4.5, 4H), 7.46 (s, 1H), 7.72–7.75 (m, 2H), 7.78–7.80 (m, 2H), 8.21–8.23 (m, 1H), 9.22–9.26 (m, 2H), 9.37–9.39 (m, 1H), 9.46–9.48 (dd, J = 8 and 1.5, 1H), 9.56–9.58 (dd, J = 8.5 and 1.5, 1H). ^{13}C NMR (125 MHz, CDCl$_3$): δ 53.16, 67.10, 112.80, 123.93, 124.20, 125.68, 127.35, 127.73, 127.91, 129.37, 130.20, 131.70, 133.36, 133.47, 137.15, 139.46, 139.90, 143.54, 146.68, 147.05, 151.39, 151.75, 153.26. HRMS (ESI): *m*/*z* calcd for $(M + H)^+$ $C_{26}H_{19}N_5O$ 418.1662; found 418.1650

2.3.5.3. 4-(Acenaphtho[1′,2′:5,6]pyrazino[2,3-f][1,10]phenanthrolin-12-yl)morpholine (9). Compound **9** was synthesized by following the general procedure described above 1, 10-phenanthroline-5, 6-diamine (0.23 g, 1.12 mmol) and intermediate 8 (0.3 g, 1.12 mmol) refluxed in methanol. (Yield: 0.28 g, 57.57%). Melting point >300 °C. ^{1}H NMR (500 MHz, CDCl$_3$): δ 3.41 (t, 4H), 4.08 (t, 4H), 7.23–7.25(d, J = 7.5, 1H), 7.79–7.82 (m, 3H), 8.23–8.25 (d, J = 8.5, 1H), 8.34–8.35 (d, J = 7, 1H), 8.43–8.45 (d, J = 7.5, 1H), 9.27 (m, 2H), 9.66–9.69 (t, J = 7, 2H). ^{13}C NMR (125 MHz, CDCl$_3$): δ 53.51, 66.73, 112.01, 114.30, 116.60, 118.89, 122.35, 123.26, 126.53, 128.32, 129.39, 134.25, 135.51, 135.90, 136.96, 137.16, 137.52, 137.87, 152.58, 152.74, 153.84. HRMS (ESI): *m*/*z* calcd for $(M + H)^+$ $C_{28}H_{19}N_5O$ 442.1662; found 442.1631.

2.3.5.4. 4-(Dibenzo[a,c]dipyrido[3,2-h:2′,3′-j]phenazin-12-yl)morpholine (13). Compound **13** was synthesized by following the general procedure described above phenanthroline-5, 6-diamine (0.21 g, 1.023 mmol) and compound **8** (0.3 g, 1.023 mmol) were refluxed in methanol. (Yield = 0.220 g, 46.02%). Melting point >300 °C. ^{1}H NMR (500 MHz, CDCl$_3$): δ 3.20 (t, 4H), 3.87 (t, 4H), 6.55–6.57 (d, J = 7.5, 1H), 6.76 (s, 1H), 7.20–7.27 (m, 2H), 7.64–7.85 (m, 4H), 8.19–8.20 (d, J = 4.5, 1H), 8.68–8.69 (d, J = 6, 1H), 8.79–8.81 (d, J = 6, 1H), 8.98–9.00 (m, 2H). HRMS (ESI): *m*/*z* calcd for $(M + H)^+$ $C_{30}H_{21}N_5O$ 468.1819; found 468.1800.

3. Result and discussion

3.1. Discussion of synthesis

Synthesis of compounds **4** and **5** were accomplished by reacting N, *N*-diethyl aniline and morpholine with intermediate 1 in methanol-water mixture and in neat water respectively. Michael addition reaction of morpholine with α, β unsaturated ketone was found much easier in the presence of sulfonate salt. After the addition of morpholine to the slightly wet sulfonate salt red colored intermediate **3** was formed immediately, and after a span of 24 h at room temperature black colored intermediate **2** was formed [66,75–77]The intermediates **2** and **3** were treated with 1, 10-phenanthroline-5, 6-diamine in methanol at reflux condition for 5–6 h to obtain the desired compounds **4** and **5** respectively (Scheme 1). 1, 10-Phenanthroline-5,6-diamine was synthesized by following the reported procedure [78]. Intermediates **7** and **11** were

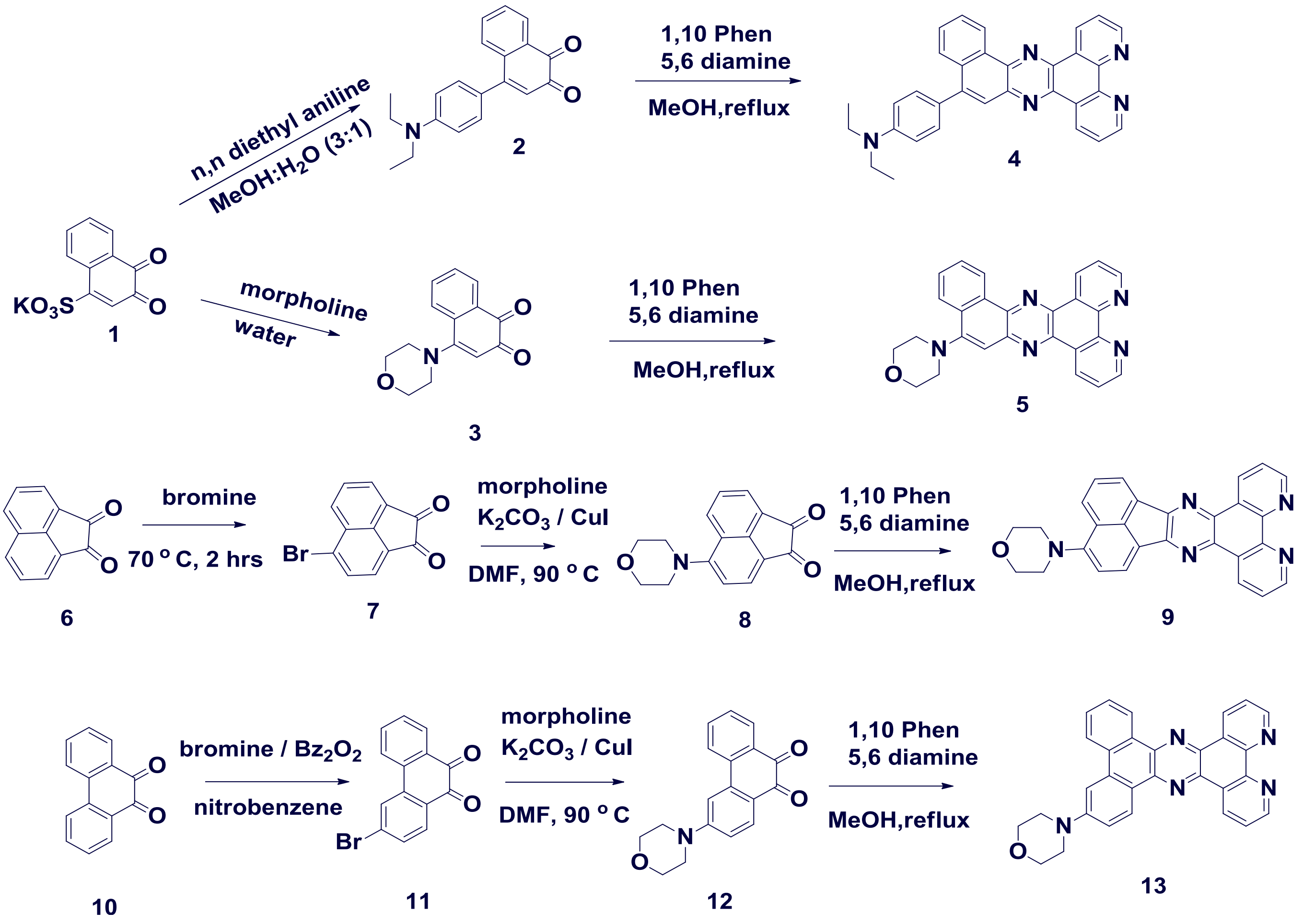

Scheme 1. Synthetic route for compounds **4, 5, 9** and **13**.

synthesized by following the reported procedure [68,69] and treated with morpholine using potassium carbonate and cuprous iodide as catalyst in N, *N*-dimethylformamide (DMF) as solvent at 90 °C for 4–5 h to obtain the reddish colored intermediate **8** and **12** respectively. The crude products were purified by column chromatography and further treated with 1, 10-phenanthroline-5, 6-diamine to obtain the desired compounds **9** and **13** respectively (Scheme 1). Compounds **4, 5** and **9** were isolated as pure products. Compound **13** was further purified by column chromatography. All the four compounds **4, 5, 9** and **13** were characterized by ^{1}H NMR, ^{13}C NMR and HR-LCMS analysis. Due to extra nitrogen atoms these compounds are quite insoluble in $CDCl_3$ and also precipitated out from DMSO-d_6, hence we added very slight deuterated TFA to complete ^{1}H NMR analysis except compound **5** which shows very good solubility in common organic solvents. All the compounds are yellow to reddish in color and shows optimum to very good solid state fluorescence.

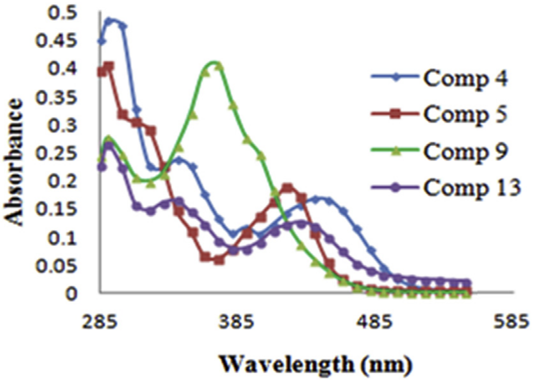

Fig. 2. Comparative absorption spectra of compounds **4, 5, 9** and **13.**

3.2. Photophysical properties

Absorption spectra of all the four compounds were recorded in chloroform using their 10 μM solutions as shown in Fig. 2 and related photophysical parameters are compiled in Table 1. All the compounds exhibited very broad absorption spectra with at least two distinct absorption maxima. The lowest energy transition around 420–450 nm is mainly due to the charge transfer (CT) band originating from the HOMO of morpholine donor and LUMO of pyrazine acceptor supported with two more accepting electron of rigid phenanthroline moiety. In compound **4** and **13** the second lowest energy π-π transition peak observed at 340 nm can be explained on the basis of their extended conjugation through extra phenyl ring, which is not present in compound **5** and hence shows single absorption peak at 422 nm. Comparatively blue shifted and sharp absorption peak around 365 nm with shoulder peak around 400 nm is observed for compound **9** is mainly due to the higher energy required for the electrons to navigate around the acenaphthene structure. This derivative especially enclose one more

Table 1
Photophysical parameters of compound **4, 5, 9** and **13** before and after the addition of TFA.

Compound	λ_{abs} (nm)	ε_{max} x 10^4 (M^{-1} cm^{-1})	fwhm (nm)	λ_{ems} (nm)	Stokes shift		Φ_F	λabs (Comp + TFA) (nm)	(ε_{max} x 10^4) (Comp + TFA) (M^{-1} cm^{-1})	$K_r \times 10^8$ (S^{-1})
					(nm)	(cm^{-1})				
4	341	2.32	39	–	259	12658	–	–	–	1.85
	444	2.13	81	600	156	5855	0.154	417	1.9	1.51
5	424	1.79	101	525	101	4537	0.91	538	1.47	1.11
9	364	4.37	110	539	175	8920	0.071	332	4.55	3.15
13	334	2.94	59	–	197	11108	–	–	–	2.94
	421	2.28	65	531	110	4920	0.421	404	3.09	2.28

extra five membered ring which makes the structure again more tight to show sharp absorption peak with highest molar extinction coefficient [45]. The third and highly energetic transition around 300 nm for all four compounds consists of various vibrational components of the same π-π electronic transition. Among all the four compounds the highest molar extinction coefficient is observed for compound **9** while the lowest one is for compound **13**. Similarly due to its extended conjugation and effective *N,N* diethyl aniline donor compound **4** shows absorption maxima at the longest wavelength among all the four compounds. To gain further insight into the photophysical process of these donor-acceptor compounds we investigated the absorption and emission behavior of compounds **4, 5, 9** and **13** in different solvents. Slight red shift in absorption spectra after increasing solvent polarity (Fig. S2-S4) indicates that negligible intramolecular interaction between donor and acceptor groups is present in the ground state.

Similarly as represented in Fig. 3 emission spectra of these compounds were studied using their 10 μM solutions in chloroform. These are yellowish-orange bright fluorescent compounds showing broad emission spectra starting from 500 nm and extending up to 700 nm as shown in Fig. 3. As cited in Table 1, compound **5** shows maximum fluorescence quantum yield as compared to the other derivatives i.e. compound **4**, compound **9** and compound **13**, mainly due to the effective charge transfer from donor to acceptor pyrazine ring and compound **4** is showing red shifted emission among all four compounds due to its the longest conjugation length between the donor *N N* diethyl aniline and acceptor pyrazine moiety. The normalized absorption as well emission spectra for all the four compounds is represented in Fig. S1. Photophysical parameters like full width half maximum (FWHM), molar extinction coefficient, Stokes shift, quantum yield, oscillator strength (f), transition dipole moment (μ_{eg}), radiative and non-radiative rate constant (Kr and Knr) and fluorescence lifetime (τ) of all the four compounds in different non-polar to polar solvents were evaluated and represented in Table 2 and Table S1-S3.

As two prominent absorption peaks were observed for compounds **4** and **13** we calculated all the parameters related to both of these absorptions and it is observed that for both the compound particularly low energy absorption maxima is related with the maximum FWHM, radiative rate constant and fluorescence lifetime in all the solvents.

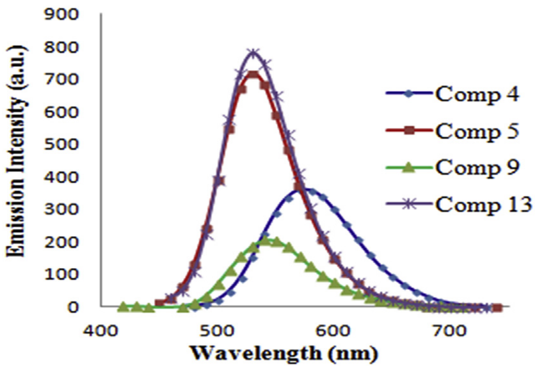

Fig. 3. Comparative emission spectra of compounds **4, 5, 9** and **13.**

A value for transition dipole moment has been calculated which is a measure of the probability of radiative transitions from ground to excited state and correlated to the oscillator strength as represented in equation (1)

$$\mu_{ge} = 2.13 \times 10^{-30} \frac{f}{\bar{\nu}} \tag{1}$$

where f = oscillator strength and $\bar{\nu}$ = absorption wave number in cm^{-1}

Oscillator strength (f) is expressed as

$$f = 4.32 \times 10^{-9} \int \varepsilon(\bar{\nu}) d\bar{\nu} \tag{2}$$

and can be obtained by integrated absorption coefficient.

For all the four derivatives from non polar to polar solvent quenching of fluorescence resulted into the lowering of quantum yield and red shifted emissions are observed. Due to its unique rigid structure compound **9** shows highest values of molar extinction coefficient, FWHM, Stokes shift, oscillator strength and transition dipole moment among all the four derivatives, while compound **5** shows highest values of quantum yield, fluorescence lifetime and minimum non-radiative decay constant among all the four derivatives as expressed by Strickler Berg equation

$$Kr = 2.88 \times 10^{-9} n^2 \bar{\nu}_{av}^2 \int \varepsilon_{\bar{\nu}} d\nu \tag{3}$$

where $\bar{\nu}_{av}$ is the average wave number corresponding to the 0–0 transition and the integral part is evaluated from the area under the curve of absorption and emissions in all solvents.

Compound **9** shows highest values of radiative as well as non-radiative rate constants in all four derivatives. After knowing the values of observed quantum yield, fluorescence lifetime (τ) can be calculated using equation (4)

$$\mathrm{T} = \Phi F/\mathrm{Kr} \tag{4}$$

As fluorescence lifetime is directly proportional to observed quantum yield, compound **5** shows highest fluorescence lifetime while compound **9** shows lowest one among all the four derivatives. By knowing fluorescence lifetime non-radiative decay constant is calculated using equation (5)

$$Knr = (1 - \Phi F)/\tau \tag{5}$$

Compound **4** and **5** show lower value of non-radiative decay constant (Knr) than their corresponding radiative decay constant (Kr) in all solvents, while in the case of compound **9** and **13** the

Table 2
Photophysical parameters of compound **4** in all solvents.

Solvent	λ_{abs} (nm)	$\varepsilon_{max} \times 10^4$ (M^{-1} cm^{-1})	fwhm (nm)	λ_{ems} (nm)	Stokes shift (nm)	Stokes shift (cm^{-1})	Φ_F	f	TDM (debye)	$K_r \times 10^8$ (S^{-1})	$K_{nr} \times 10^8$ (S^{-1})	τ (ns)
Comp 4												
Dioxane	441	2.72	79	530	135	5314	0.571	0.38	6.02	1.31	0.04	7.45
Toluene	443	2.27	79	514	109	4457	0.734	0.33	5.59	1.48	0.07	6.38
Chloroform	444	2.13	81	526	156	5855	0.154	0.34	5.68	1.51	0.14	6.04
EtOAc	441	2.32	87	545	181	6598	0.046	0.35	5.79	1.14	0.15	7.66
THF	447	2.38	80	541	183	6498	0.035	0.34	5.75	1.17	0.24	7.06
Acetone	442	2.47	90	559	99	4140	0.004	0.35	5.74	1.01	0.96	5.07
MeOH	445	2.17	98	572	130	5080	0.022	0.4	6.18	1.15	0.34	6.66
Acetonitrile	442	2.24	94	559	116	4703	0.034	0.36	5.88	0.99	0.24	8.05
DMSO	456	2.57	97	584	116	4447	0.062	0.42	6.4	1.31	0.37	1.97

Dielectric constant (Є) of solvents = Dioxane (2.25), Toluene (2.38), Chloroform (4.81), EtOAc (6.02), THF (7.58), Acetone (20.7), MeOH (32.7), Acetonitrile (37.5), DMSO (46.7). Where EtOAc = Ethyl acetate, THF = Tetrahydrofuran, MeOH = Methanol and DMSO = Dimethyl sulfoxide.

values of Knr are higher than that of the Kr in respective solvents. In polar solvents the value of Knr increases for all the four derivatives.

3.3. *Acidochromism*

On protonation of nitrogen based heterocycles such as pyridine, pyrazine by using organic acids such as trifluoroacetic acid a dramatic red shift in absorption spectra is already reported [66]. In our case we observed red as well as blue shifted absorption spectra on the addition of 1–1000 eq of trifluoroacetic acid as represented in Fig. 6.

In the case of compound **5** (Fig. 4), on addition of 10 eq of TFA into 10 μM solution of the compound in toluene initially slight red shifted peak at 434 nm was observed instead of original absorption peak at 422 nm which was further replaced by totally new red shifted absorption peak at 537 nm with shoulder peak at 446 nm and 360 nm when up to 1000 eq of TFA was added into the solution. This red shifted absorption peak observed on the addition of TFA is represented as positive acidochromism and is mainly attributed to the positively charged protonated segment of intermediate A as shown in Scheme 2. A strong charge transfer from the electron rich morpholine donor to the electron deficient positively charged pyrazine acceptor is possible (intermediate **A**) which may be converted to highly protonated species (intermediate **B**) in Scheme 2 on addition of excess TFA and no further enhancement in absorption λmax is observed. In the case of remaining compounds **4, 9** and **13** instead of protonation at pyrazine segment the nitrogen atom of the morpholine donor may have protonated initially to form intermediate **C** to afford the blue shifted absorption λmax. The protonated intermediate **C** may not be showing effective charge transfer causing blue shifted absorption spectra after the addition of very small quantity of TFA and hence a negative acidochromism. On addition of excess TFA highly protonated intermediate **D** may have formed showing no further enhancement in molar extinction coefficient. On addition of TFA, compound **9** shows a new absorption peak at 332 nm (Fig. 5), while compounds **4** and **13** show new peak at 417 and 402 nm (Fig. S11 and S12). The absorption spectra observed for all the four compounds before and after the addition of TFA are represented in Fig. 6.

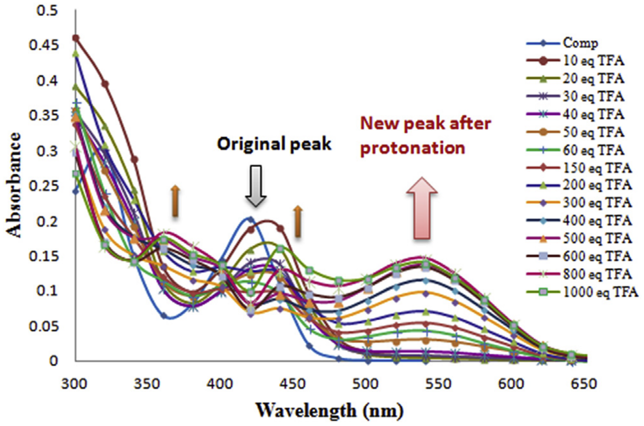

Fig. 4. Positive acidochromism absorption spectra observed for compound **5** after the addition of different amount of TFA.

3.4. *Solvatochromism*

In the case of donor-acceptor compounds the polarity of solvents strongly affects the excited state of the molecule by stabilizing it through dipole-dipole, hydrogen bonding, and solvation interactions (see Fig. 7). Hence we studied the solvent dependent absorption as well as emission behavior of these compounds in solvents of different dielectric constants. In polar solvents such as chloroform, MeOH, acetonitrile and DMSO all the compounds showed a less pronounced red shift in their absorption spectra and a very large red shift in their emission spectra particularly in polar solvents, indicating that the excited state is highly polar as compared to the ground state, resulting in a stronger interaction of polar solvents in the excited state and causing red shifted emissions. These observations are further supported by the more positive difference in dipole moment of the ground and excited state (i.e. $\mu_e > \mu_g$) and increased Stokes shift in polar solvents as compared to the non-polar solvents (Table 2 and Tables S1-S3). The normalized emission spectrum of compound **13** is shown in Fig. 8 indicates the highest shift in emission spectra (98 nm) from non-polar to polar solvent. Compound **4, 5** and **9** show a red shift of 70, 52 and 58 nm in their emission spectra respectively.

Solvatochromism observed in these compounds with gradual increase in Stokes shift with increase in the solvent polarity can be correlated by using Lippert-Mataga equation [79]. Lippert- Mataga equation is showing direct correlation of physical parameters of solvent i.e. dielectric constant, refractive index and change in dipole moment of the compound upon excitation with Stokes shift.

$$\text{Stokes shift} = \vartheta abs - \vartheta ems$$

$$= \left[\frac{2\left(\mu_e - \mu_g\right)^2}{hca^3}\right] \Delta fLM + \text{constant}\ldots \qquad (6)$$

where ν_{abs} and ν_{ems} are absorption and emission expressed in

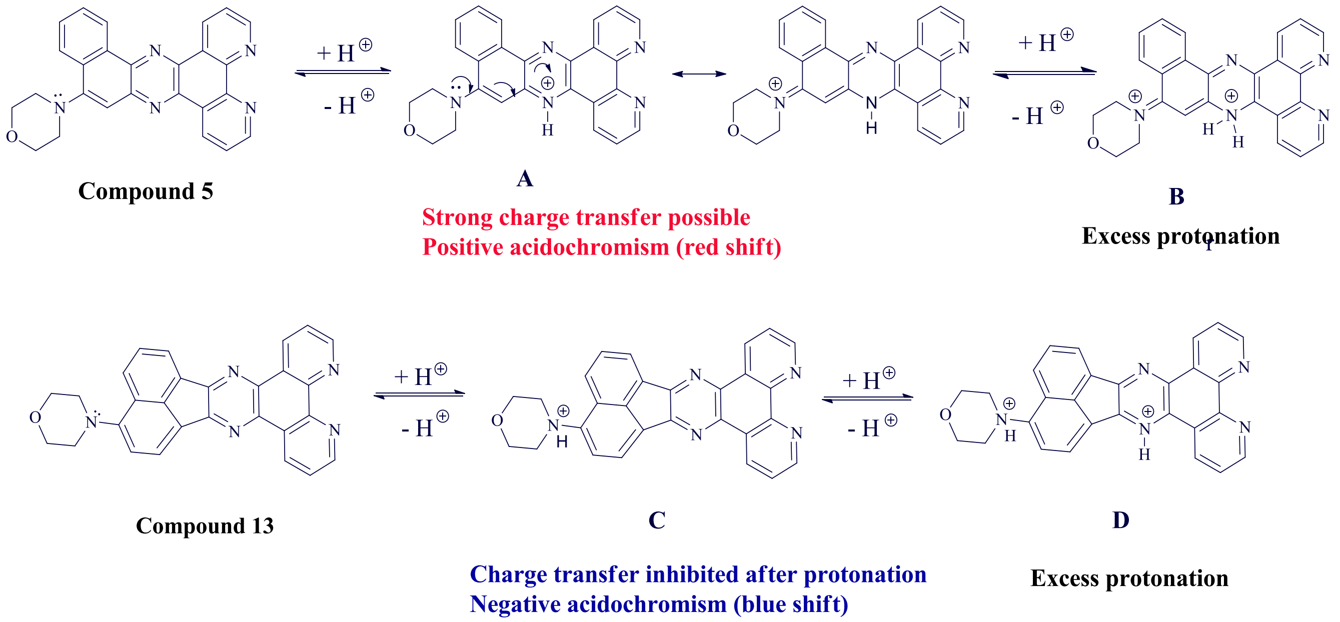

Scheme 2. Protonation-Deprotonation mechanism of compound **5** and **13** after the addition of TFA.

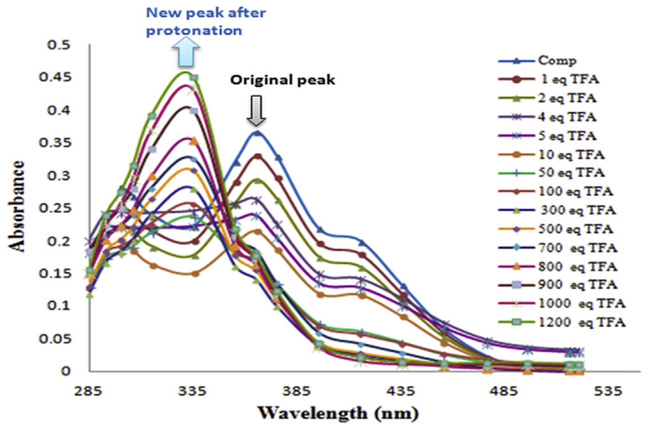

Fig. 5. Negative acidochromism absorption spectra observed for compound **9** after the addition of different amount of TFA.

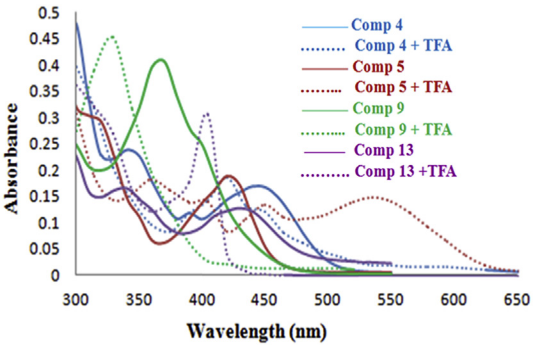

Fig. 6. Combined absorption spectra for compound **4, 5, 9** and **13** before and after the addition of TFA.

cm^{-1},h = Planck's constant,c = velocity of light in vacuum,a = radius of the solvent cavity in which the fluorophore resides (Onsager cavity radius),μ_g = ground-state dipole moment

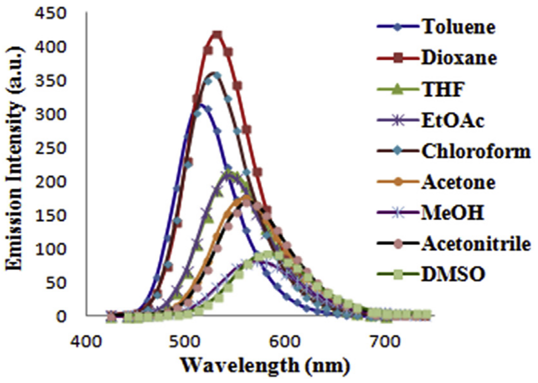

Fig. 7. Emission spectra of compound **5**.

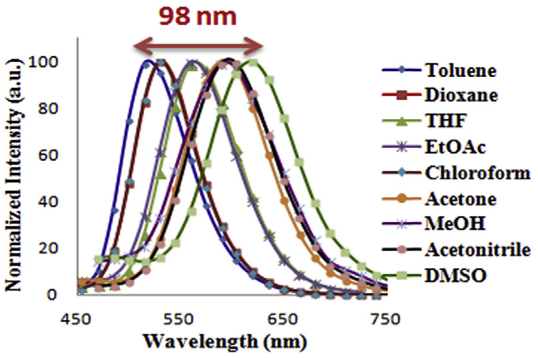

Fig. 8. Normalized emission spectra of compound **13**.

andμ_e = excited state dipole moment.

Δf_{LM} = Lippert-Mataga function, also called as orientation polarizability.

It is a very general equation for the effect of solvent on emission properties and does not account for specific solvent—fluorophore interactions, e.g. hydrogen bonding. The plot of Stokes shift vs orientation polarizability (Lippert-Mataga function) exhibited linear relationship (Fig. 9) suggesting that solvent parameters such as dielectric constant and refractive index are collectively responsible for the red shift in emission. In addition, these compounds also show different types of interactions with polar and non-polar solvents. A linear relationship with polar solvents such as DMSO, acetonitrile, methanol and acetone is due to the dipole-dipole relaxation. Similarly linear relationship between non polar solvents such as toluene and dioxane is observed. Also there is no specific hydrogen bonding effect observed as protic solvent methanol is showing linear behavior with Stokes shift.

As Mac Rae is the improved version of Lippert-Mataga where solute polarizability in addition to the solvent polarizability is also taken into account [80], we plotted the Mac Rae function(Δf_{MR}) vs Stokes shift plots for all four derivatives in different solvent as shown in Fig. S9 and found linear relationship which suggests that the polarity originating from the dipole created by these dyes also contributed to the solvatochromic shift observed in polar solvents.

It is correlated with the Stokes shift as

$$\text{Stokes shift} = \left[\frac{2\left(\mu_e - \mu_g\right)^2}{hca^3}\right]\Delta f\mathrm{MR} + \text{constant}\ldots \tag{7}$$

where, Mac Rae function (Δf_{MR}) is defined as

$$\Delta f\mathrm{MR} = \left[\frac{\varepsilon - 1}{\varepsilon + 2}\right] - \left[\frac{\mathbf{n}^2 - 1}{\mathbf{n}^2 + 2}\right]$$

where ε = Dielectric constant andn = Refractive index.

Similarly molecular-microscopic solvent polarity parameter (E_T^N) introduced by Reichardt [81,82] which correlates much better with the solvatochromic shift of dipolar molecules rather than the traditionally used bulk solvent polarity functions (for e.g. Lippert-Mataga) is also plotted with the Stokes shift and linear relationship is observed as shown in Fig. S10.

3.5. Multilinear regression analysis using Kamlet-Taft and Catalan parameters

The solvent dependent spectral shift observed for organic compounds is well explained by single-parameter scales like Lippert-Mataga, Mac-Rae, (E_T^N) and other similar solvent parameters, but it is found that these parameters are inappropriate to explain exactly which solvent property or solute-solvent interaction is responsible for the observed solvent dependent physiochemical changes. Therefore a multi-parameter approach is preferred and has been successfully applied to various physiochemical processes for e.g., UV-Visible absorption spectra, emission maxima in fluorescence spectra, Stokes shifts, quantum yield, radiative and non-radiative rate constants and fluorescence life time, etc.

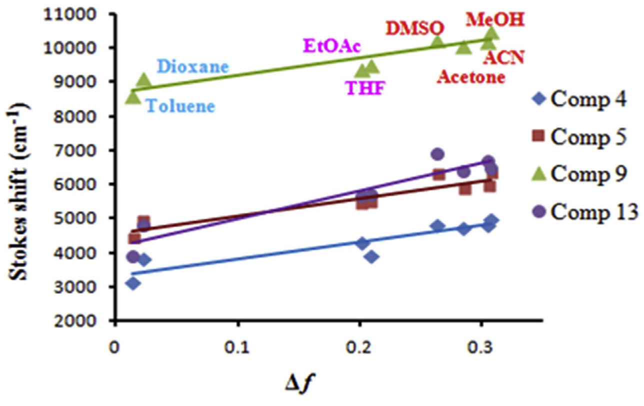

Fig. 9. Lippert-Mataga correlations between stokes shift and orientation polarizability (Δf).

In general the multi-linear expression is given as

$$y = y_0 + aA + bB + cC + dD\ldots \tag{8}$$

where y is the solvent affected physiochemical property, y_0 stands for the studied physiochemical property in the gas phase. When all other solvent parameters are absent, then $y = y_{0.}$ a, b, c and d are adjustable coefficients which reflect the dependence of y to the various {A, B, C, D} solvent parameters. In this paper we studied three different physiochemical properties (y) namely absorption maxima ($\bar{\upsilon}_{abs}$), emission maxima ($\bar{\upsilon}_{emi}$) and Stokes shift ($\Delta\bar{\upsilon}$). The solvent effects are divided into two main categories namely (a) specific interactions for e.g. localized donor-acceptor interactions which involves specific orbitals and acid-base interactions which involves hydrogen bonding. (b) Non-specific interactions originated from solvents which act as dielectric continuum. Though there are different solvent scales available in the literature, those provided by Kamlet and Taft [83,84] is most frequently used and expressed as …

$$y = y_0 + a_\alpha \alpha + b_\beta \beta + c_{\pi*} \pi* \ (\text{Kamlet} - \text{Taft}) \tag{9}$$

where α represents effect of acidity (hydrogen-bond donating ability) of solvent, β represents effect of basicity (hydrogen-bond accepting ability) of solvent and π^* represents the collective effect of solvent polarity (also known as dipolarity) and polarizability. But if acidity or basicity of solvents is not affecting on the value of y, then among polarity and polarizability it is difficult to sort out which factor is exactly influencing the studied physiochemical property y, hence Catalan [85–87] proposed another expression …

$$y = y_0 + a_{SA}SA + b_{SB}SB + c_{SP}SP + d_{SdP}SdP \ (\text{Catalan}) \tag{10}$$

where instead of three, total four solvent parameters namely SA (solvent acidity), SB (solvent basicity) SP (solvent polarizability) and SdP (solvent dipolarity) were introduced where the newly introduced parameter SdP can make difference between the exact contribution of solvent polarizability (SP) and solvent dipolarity (SdP). Also the individual solvatochromic parameters explained by Catalan are based on well-defined reference processes as opposed to the Kamlet-Taft parameters which are based on the average of several solvent-dependent processes. Since the Kamlet-Taft parameters are well established and Catalan parameters are the improved and modified version of it, we used both these approaches simultaneously to understand exactly which factor is mostly affecting the slightly blue shifted absorption spectra, red shifted emission spectra and increased Stokes shift in polar solvents of four pyrazine based fused donor-acceptor π-conjugated compounds in solvents of different acidity, basicity or polarity. The Kamlet-Taft parameters [88] and Catalan parameters [89] were taken from the literature.

Multi-linear analysis of absorption maxima ($\bar{\upsilon}_{abs}$), emission maxima ($\bar{\upsilon}_{emi}$) and Stokes shift ($\Delta\bar{\upsilon}$) for compound **4** in nine different sets of solvents were carried out by using both Kamlet-Taft (2) and Catalan (3) parameters (Table 3). Analysis of absorption spectra ($\bar{\upsilon}_{abs}$) of compound **4** in different solvents shows comparatively higher correlation coefficient (0.91) obtained by Catalan

Table 3
Estimated coefficients (y_0, a, b, c, d), their standard errors and correlation coefficients (r) for the multi-linear analysis of ($\bar{\upsilon}_{abs}$), ($\bar{\upsilon}_{emi}$) and ($\Delta\bar{\upsilon}$) of compound **4** as a function of Kamlet-Taft (2) and Catalan (3) solvent scales. Where, α or SA for solvent acidity, β or SB for solvent basicity, π* for collective parameter of solvent dipolarity and polarizability according to Kamlet-Taft equation, SdP and SP for solvent dipolarity and polarizability respectively according to Catalan equation.

Kamlet-Taft	$y_0 \times 10^3$	a_α	b_β	c_{π^*}		r
$\bar{\upsilon}_{abs}$	23.18 ± 0.31	0.02 ± 0.24	−0.26 ± 0.44	−0.89 ± 0.61		0.34
$\bar{\upsilon}_{emi}$	20.72 ± 0.41	−0.74 ± 0.31	−1.60 ± 0.57	−2.54 ± 0.79		0.89
$\Delta\bar{\upsilon}$	8.15 ± 1.21	−1.20 ± 0.92	3.05 ± 1.69	−6.22 ± 2.35		0.34
Catalan	$y_0 \times 10^3$	a_{SA}	b_{SB}	c_{SdP}	d_{SP}	r
$\bar{\upsilon}_{abs}$	25.08 ± 0.30	−0.34 ± 0.14	−0.46 ± 0.13	−0.42 ± 0.11	−2.91 ± 0.37	0.91
$\bar{\upsilon}_{emi}$	21.06 ± 0.82	−0.58 ± 0.40	−1.42 ± 0.36	−2.01 ± 0.29	−1.04 ± 1.03	0.93
$\Delta\bar{\upsilon}$	7.78 ± 4.78	−0.43 ± 2.35	1.33 ± 2.15	−1.60 ± 1.72	−2.75 ± 6.00	−0.55

method than the one obtained by Kamlet-Taft method (0.31). Very high standard error and low correlation coefficient observed for solvent acidity factor suggest that it is not playing any prominent role for the change in absorption spectra in different solvent polarities but at the same time no conclusive results are obtained for remaining three factors also. Analysis of emission spectra ($\bar{\upsilon}_{abs}$) of compound **4** also shows better results by Catalan method ($r = 0.93$) than Kamlet-Taft method ($r = 0.89$). By plotting the individual plots with each factor and seeing the correlation coefficients it can be concluded that solvent basicity (b_{SB}) is the main factor responsible for the shift in emission spectra along with the little contribution from solvent polarity and polarizability factor while the role of solvent acidity factor is totally absent. For the absorption spectra of compound **5**, after overlooking the values of four solvatochromic parameters obtained by both the methods (Table S4) and higher correlation coefficient obtained by Catalan method (0.83) than by Kamlet-Taft method (0.21), it can be predicted that solvent polarizability (d_{SP}) is the main factor affecting the absorption spectra, which was further confirmed by the plot of absorption values ($\bar{\upsilon}_{abs}$) with each individual solvent parameter. For emission spectra of compound **5,** again Catalan parameters show more conclusive results than the Kamlet-Taft parameters. All the negative values obtained for all the solvent parameters (except d_{SP}) support the red shift observed in emission spectra from non-polar to polar solvents. By plotting emission frequencies ($\bar{\upsilon}_{emi}$) with individual solvent parameters it can be concluded that the solvent dipolarity parameter (c_{SdP}) obtained by Catalan method followed by the solvent basicity parameter (b_{SB}) obtained by Kamlet-Taft method are the main factors responsible for the red shift in emission spectra while the remaining two factors are not contributing at all.

In the case of compound **9** solvent polarizability is the main factor which affects the absorption spectra, while solvent dipolarity (c_{SdP}) followed by solvent basicity (b_{SB}) are the main factors responsible for the red shifted emission spectra (Table S5). Here, estimated coefficients observed for the emission spectra show more conclusive results than that observed for the absorption spectra by both Kamlet-Taft and Catalan method. For compound **13,** estimated coefficients observed for absorption data ($\bar{\upsilon}_{abs}$) show very poor fit of multi-linear analysis by both Kamlet-Taft and Catalan method (Table S6); hence these methods may be inappropriate to explain the observed experimental results. In contrast to this, emission frequencies ($\bar{\upsilon}_{emi}$) show very good multi-linear fit by both the methods where again Catalan parameters show better results ($r = 0.96$) than Kamlet-Taft ($r = 0.75$). More negative value of estimated coefficient c_{SdP} with minimum standard error suggests that solvent dipolarity is the main factor which affects the emission spectra. The graph plotted for predicted emission data obtained by Catalan method with the experimental data for compound **4, 5, 9** and **13** shows very good linear fit with slope of 0.93, 0.95, 0.93 and 0.98 respectively (Fig. 10). In short, it is concluded that solvent polarizability is mainly responsible for the slightly blue shifted absorption spectra of compound **5** and **9**, while no conclusive results were obtained for compound **4** and **13**. In the case of emission spectra, for compound **5, 9** and **13** solvent dipolarity factor is mainly responsible and for compound **4** combinations of solvent basicity factor obtained by Kamlet-Taft method and solvent dipolarity factor obtained by Catalan method is mainly responsible for the red shifted emission spectra. Other two factors i.e. solvent acidity and polarizability are really not playing any prominent role for the observed red shift in emission spectra.

3.6. Intramolecular charge transfer (ICT) and difference in dipole moment between ground and excited state

It is well known that in the case of strong donor-π-acceptor compounds intramolecular charge transfer occurs upon excitation and this process becomes environment sensitive e.g. red shift in emission λmax observed after increasing solvent polarity. Large Stokes shift observed for these compounds also suggest a sufficient structural reorganization or a polarized excited state as compared to the ground state. For the better understanding of the polar excited state we calculated the difference in dipole moment between the ground and excited state by using Lippert-Mataga, MacRae and Reichardt correlations as represented in equations (6)–(8). Table 4 represents the transition dipole moment, difference in dipole moment by experimental and DFT method and the ratio of dipole moment using Bilot-Kawaski, Bakhshiev and Liptay correlations. Also a value for transition dipole moment has been calculated which is a measure of the probability of radiative transitions from ground to excited state and related to the oscillator strength as represented in equation (1). Much positive values obtained for the difference in dipole moment ($\mu_e > \mu_g$) as well as ratio of dipole moment (μ_e/μ_g) by experimental as well as DFT method confirmed that the excited state is highly polar than the ground state. The higher values of $\Delta\mu_{eg}$ are obtained for all the four dyes by Lippert-Mataga method because this method does not take into account the polarizability of the solute. Compound **13** is showing higher values of $\Delta\mu_{eg}$ obtained by three different correlations (i.e. Lippert-Mataga, Mac-Rae and Reichardt), while compound **5** is showing higher values of μ_e/μ_g obtained by another three different correlations (i.e. Bilot-Kawaski, Bakhshiev and Liptay). Solvent polarity effect on $\Delta\mu_{eg}$ is also studied and represented in Table S7; slight increase in the values of Δμeg is observed after moving from non-polar to polar solvent.

3.7. Electrochemical properties

Cyclic voltametry study of these dyes was carried out to understand their redox behavior. The measurements were performed in dichloromethane using tetra-*n*-butylammonium hexafluorophosphate (NBu_4PF_6) as electrolyte and ferrocene as reference standard at a scan rate of 100 mV/s. The recorded cyclic

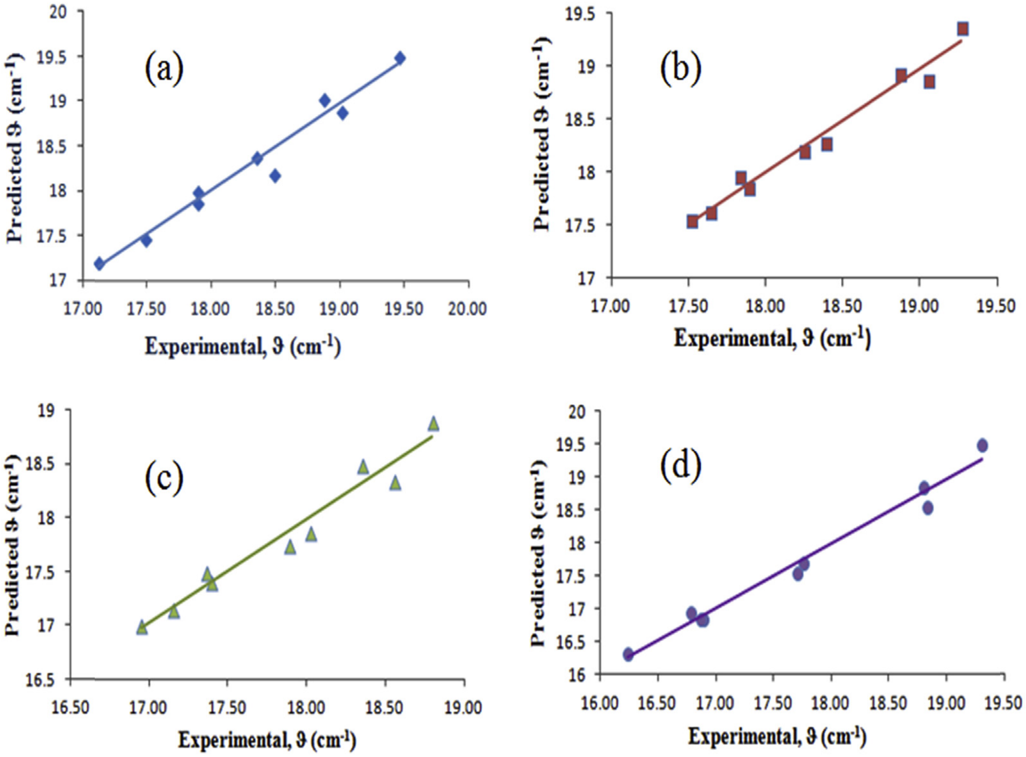

Fig. 10. Correlation between experimental and predicted emission wave number for **4**(a), **5**(b), **9**(c) and **13**(d) by Catalan method.

Table 4
Difference and ratio of dipole moment between ground and excited state of compound **4, 5, 9** and **13** by experimental as well as DFT method.

Dye	μ_{eg} (Debye)	$\Delta\mu_{eg}$ (Debye)			$\Delta\mu_{eg}$(DFT) (Debye)	μ_e/μ_g (Debye)		
		Lippert-Mataga	Mac-Rae	Reichardt		Bilot-Kawaski	Bakhshiev	Liptay
4	5.59	11.2	8.2	5.71	0.65	4.58	5.30	5.81
5	5.06	10.0	6.5	4.98	1.52	10.97	15.21	18.01
9	8.91	10.6	7.0	5.37	2.47	9.88	14.26	18.75
13	5.2	13.8	9.0	7.14	1.39	8.65	10.67	11.24

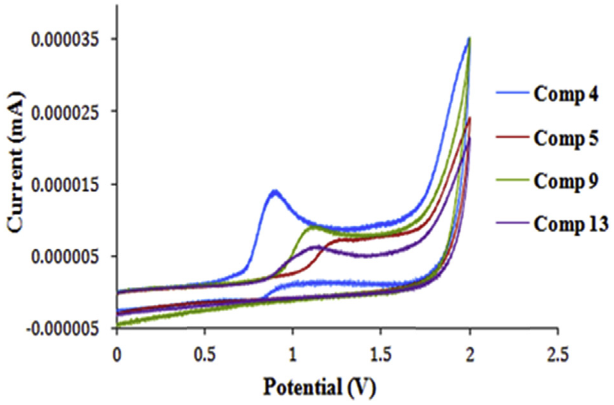

Fig. 11. Cyclic voltammograms of compound **4**, **5**, **9** and **13** in DCM at room temperature.

voltammograms are displayed in Fig. 11. These compounds show oxidation peak corresponding to the removal of an electron from the donating amine side nitrogen. As acceptor pyrazine fragment attached with supporting phenanthroline is same in all four dyes, the donating ability of morpholine or N, *N*-diethyl aniline, conjugation length between the donor-acceptor and structural effect strongly alters the oxidation potentials of these dyes. Due to the effective conjugation between donor and acceptor, compound **4** shows low oxidation potential (−0.881 mV/s) as well as lowest band gap (2.315 eV). Due to the rigid structure of compound **9**, the donor morpholine fragment is not reacting properly with the acceptor pyrazine and shows the highest band gap in all these derivatives. Also due to its shorter conjugation length compound **5** shows the highest oxidation potential among all these derivatives. The oxidation potential trend observed for these dyes is **Comp 4** < **Comp 13** < **Comp 9** < **Comp 5**. The HOMO energies of compounds were estimated using the first oxidation potential and found in the range of 5.27–5.61 eV. The LUMO energies calculated by subtracting the HOMO energy value obtained from optical band gap and found in the range of 2.96–3.20 eV. The optical band gap is obtained by using the photophysical data of all the four dyes in DCM solvent. Similarly band gap from computational method is also represented in Table 5 and it is showing the similar trend obtained from the experimental photophysical data.

3.8. *Theoretical calculation*

To correlate our experimental finding theoretically and

Table 5
Electrochemical data of compound **4, 5, 9** and **13**.

Compound	E_{oxd} (V)	E_{HOMO} (eV)	E_{LUMO} (eV)	Band gap (eV)	Band gap (DFT) (eV)
4	0.88	−5.276	−2.961	2.315	2.769
5	1.22	−5.615	−3.204	2.411	3.425
9	1.11	−5.505	−3.018	2.487	3.442
13	1.09	−5.485	−3.101	2.384	3.231

understand molecular geometries and electronic properties of these compounds time-dependent density functional theory (TD-DFT) calculations were performed with the Gaussian 09 program using the B3LYP functional [71,72,90]. We optimized the molecular structure of these compounds in the gas phase as well as in chloroform solvent using 6-31G (d) basis set. Computations in solvent were carried out using the Polarizable Continuum Model (PCM). Gaussian 09 program was used for all the quantum mechanical computations. Fig. 12 represents optimized geometry structure of compound **4** in chloroform solvent. We found that the *N,N*-diethyl aniline unit is slightly twisted with the naphthalene core. There are significant steric interactions between the aromatic protons of the *N,N*-diethyl aniline unit and the peri-proton of thee naphthalene unit which cause the aromatic ring of the aniline unit to be twisted out of conjugation.

Variation in bond length and bond angle at ground and excited state (marked by red) is displayed to understand the flow of electronic density from donor *N,N* diethyl aniline towards acceptor pyrazine and phenanthroline ring. For example, bond length of N_{48}-C_{37} gets shortened by 0.021 A^0 while bond length of C_{20}-N_{21} is extended by 0.025 A^0 after excitation suggesting that, for effective charge transfer from donor *N,N* diethyl aniline towards acceptor pyrazine single bond to double bond and vice versa interconversion has happened when we go from ground to excited state. Also that much variation in bond length is not observed from pyrazine to phenanthroline nitrogen insisting that maximum electron density is accepted by pyrazine nitrogen and phenanthroline nitrogen is not much engaged in the charge transfer mechanism. Also slight twist in bond angle C_{30}-C_{28}-C_{29} of 1^0 is also observed from ground to excited state for the effective charge transfer from *N,N* diethyl aniline donor moiety. Fig. 14 shows their optimized molecular structures together with the frontier molecular orbital profiles displaying electronic distributions in their HOMO and LUMO in their excited state. Tables S8 to S11 represents the respective Cartesian coordinates for all the four compounds.

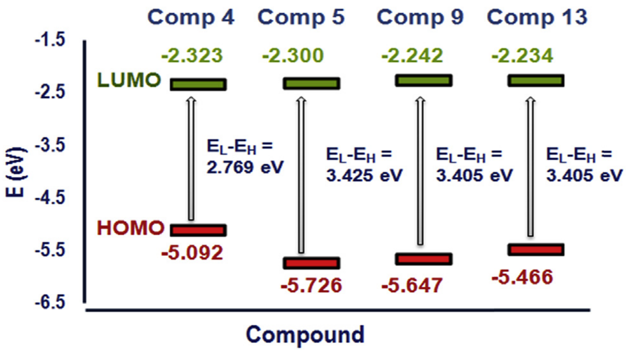

Fig. 13. HOMO-LUMO energy gaps of compounds **4**, **5**, **9** and **13** in chloroform solvent.

The energy gap between HOMO and LUMO for all the four dyes were represented in Fig. 13; as expected compound **4** shows lowest band gap (2.705 eV) due to its maximum conjugation length among all the four derivatives and compound **5** shows highest band gap (3.388 eV) due to its minimum conjugation length. It is observed that while moving from non-polar to polar solvents the energy gap gets reduced, particularly the energy of LUMO level get reduced mainly due to the stabilization of the excited state in polar solvents.

The computationally derived lowest energy transitions i.e. vertical excitations, oscillator strengths (both at ground and excited state) and emissions were compared with the experimentally observed absorptions, emissions and oscillator strength derived from absorption λmax in chloroform solvent [Table 6]. In general computationally observed vertical excitation values are well in agreement with the experimental one with percentage deviation

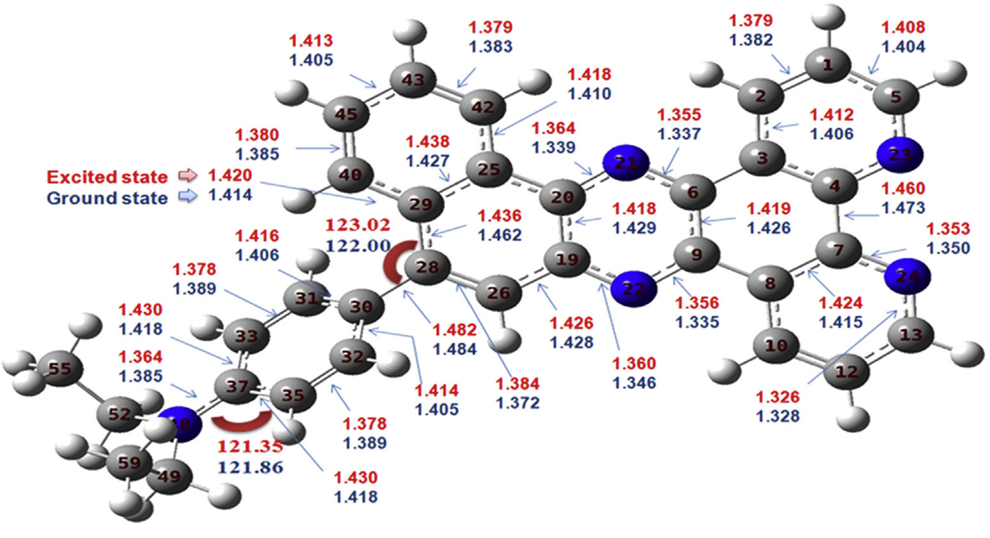

Fig. 12. Optimized geometry parameters of compound **4** in chloroform solvent at ground and excited state (bond lengths are in A^0, bond angles are in degree °).

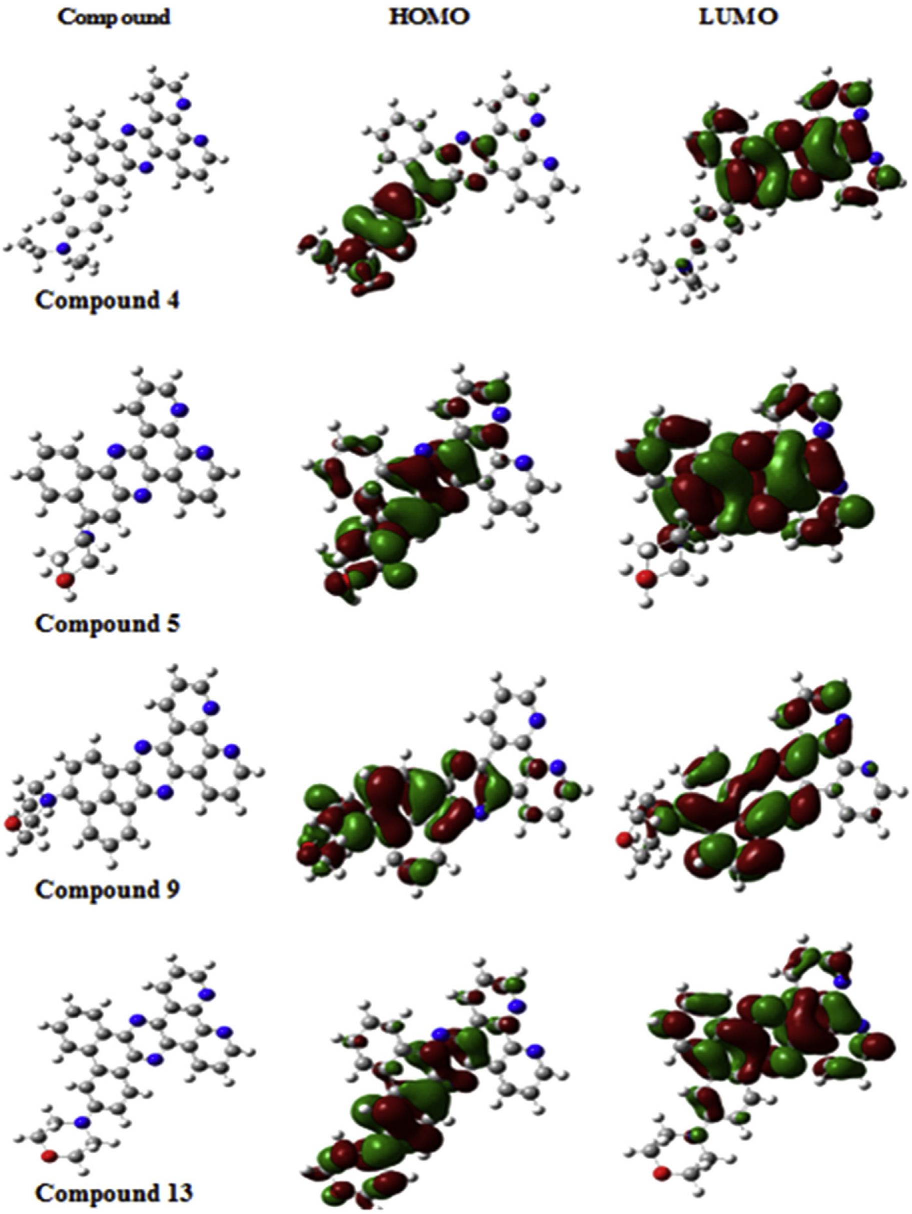

Fig. 14. HOMO-LUMO FMO diagrams of compound **4, 5, 9** and **13** in chloroform solvent at excited state.

Table 6
Comparative experimental and computational photophysical parameters of **4, 5, 9** and **13** in chloroform solvent.

Compound	Experimental/Computational absorption data						Experimental/Computational emission data				
	λabs[a] (nm)	λabs[b] (nm)	f[c]	f[d]	% D[e]	Major[f] contribution	λems[g] (nm)	λems[h] (nm)	f[i]	% D[j]	Major[k] contribution
4	444	522	0.34	0.2736	17.56	H → L 99.28	526	593	0.20	12.72	L → H 99.43
5	424	423	0.29	0.37	0.23	H → L 96.56	525	525	0.22	0.01	L → H 97.76
9	364	363	0.99	0.4808	0.27	H-1 → L 82.66	539	527	0.08	2.27	L → H 97.40
13	421	446	0.41	0.3456	5.93	H → L 97.72	531	536	0.22	0.86	L → H 98.62

[a] Experimental absorption λmax,
[b] Computational vertical excitation,
[c] Experimentally calculated oscillator strength,
[d] Theoretical oscillator strength,
[e] Percent deviation from experimental absorption λmax,
[f] Major electronic transition from ground to excited state,
[g] Experimental emission λmax,
[h] Computational emission λmax,
[i] Oscillator strength of vertical emission,
[j] Percent deviation from experimental emission λmax,
[k] Major electronic transition from excited state to ground state.

from 0 to 20%. Major contribution of electronic transitions for compound **4, 5** and **13** is from HOMO to LUMO (96–99%), while for compound **9** it is from HOMO-1 to LUMO (83%). From the HOMO-LUMO diagram of all the four derivatives (Fig. 10) it is clear that the electron density at HOMO-orbital is mainly located at donor side i.e. on N, *N*-diethyl aniline or morpholine side, while in the case of LUMO-orbital it is shifted towards acceptor pyrazine or phenanthroline segment.

Except compound **5**, all the remaining dyes show some overlap of electron densities between donor and acceptor side suggesting that the pure charge transfer is observed only in the case of compound **4** mainly due to the elongated conjugation length. This theoretical observation is well supported experimentally also as red shifted absorption and emissions were observed for this particular compound as compared to all the other derivatives. Equivalent with the electrochemical observations compound **9** is not showing good charge transfer due to its rigid structure and the electron density is not separated on donor in HOMO and on acceptor in LUMO orbital, but spread over the entire molecule. The ground state dipole moments of compound **4** are higher than any other derivative again confirming that the higher charge is located at donor side in compound **4**.

4. Conclusion

In summary we have synthesized phenanthroline based rigid donor-π-acceptor compounds to study their photophysical properties and structure property relationships. Acidochromic behavior of these dyes was studied in solution after the addition of TFA in toluene solvent and clear positive and negative acidochromism due to the protonation of nitrogen at two different reacting sites is observed and is also proved mechanistically. Very high quantum yield, positive solvatochromism and quenching of fluorescence in polar solvent observed is well supported by Lippert-Mataga, MacRae and Reichardt correlations. Also the multi-linear regression analysis utilizing Kamlet-Taft and Catalan parameters is carried out and it is concluded that in general solvent dipolarity is the main factor responsible for the observed red shifted emission spectra of all the four compounds, while solvent polarizability is responsible for the slightly blue shifted absorption spectra of compound **5** and **9**. The experimentally observed absorption and emission λ_{max} values are in good agreement with the computationally derived one. By correlating the observed difference in dipole moment between ground and excited state, band gap calculated between HOMO and LUMO, lowest oxidation potential obtained by cyclic voltametry and no overlap of energy densities observed between HOMO and LUMO frontier molecular orbitals by TD-DFT method, compound **4** is proved as highest intramolecular charge transfer dye and expected to deliver better linear and non-linear optical properties in comparison with the other derivatives studied.

Acknowledgements

Author SSK is thankful for University Grants Commission (UGC), India for a Research Fellowship. We are thankful to Mrs. Kripa Subramanian and Prof. B.M. Bhanage, Department of chemistry, ICT for the Cyclic Voltametry study. Also we are thankful to the Sophisticated Analytical Instrument Facility (SAIF), IIT, Mumbai, India for the recording of mass and HR-MS spectra.

Appendix A. Supplementary data

Supplementary data related to this article can be found at http://dx.doi.org/10.1016/j.dyepig.2016.08.032.

References

[1] Mikroyannidis JA, Tsagkournos DV, Sharma SS, Vijay YK, Sharma GD. Low band gap conjugated small molecules containing benzobisthiadiazole and thienothiadiazole central units: synthesis and application for bulk heterojunction solar cells. J Mater Chem 2011;21:4679–88. http://dx.doi.org/10.1039/C0JM03436C.

[2] Sonar P, Singh SP, Li Y, Soh MS, Dodabalapur A. A low-bandgap diketopyrrolopyrrole-benzothiadiazole-based copolymer for high-mobility ambipolar organic thin-film transistors. Adv Mater 2010;22:5409–13. http://dx.doi.org/10.1002/adma.201002973.

[3] Gadisa A, Mammo W, Andersson LM, Admassie S, Zhang F, Andersson MR, et al. A new donor–acceptor–donor polyfluorene copolymer with balanced electron and hole mobility. Adv Funct Mater 2007;17:3836–42. http://dx.doi.org/10.1002/adfm.200700441.

[4] Zhang F, Bijleveld J, Perzon E, Tvingstedt K, Barrau S, Inganas O, et al. High photovoltage achieved in low band gap polymer solar cells by adjusting energy levels of a polymer with the LUMOs of fullerene derivatives. J Mater Chem 2008;18:5468–74. http://dx.doi.org/10.1039/B811957K.

[5] Lindgren LJ, Zhang F, Andersson M, Barrau S, Hellström S, Mammon W, et al. Synthesis, characterization, and devices of a series of alternating copolymers for solar cells. Chem Mater 2009;21:3491–502. http://dx.doi.org/10.1021/cm802949g.

[6] Zhou E, Cong J, Tajima K, Hashimoto K. Synthesis and photovoltaic properties of donor-acceptor copolymers based on 5,8-dithien-2-yl-2,3-diphenylquinoxaline. Chem Mater 2010;22:4890–5. http://dx.doi.org/10.1021/cm101677x.

[7] Wang E, Hou L, Wang Z, Ma Z, Hellström S, Zhuang W, et al. Side-chain architectures of 2,7-Carbazole and quinoxaline-based polymers for efficient polymer solar cells. Macromolecules 2011;44:2067–73. http://dx.doi.org/10.1021/ma102783d.

[8] Zhang Y, Zou J, Yip H-L, Chen K-S, Zeigler DF, Sun Y, et al. Indacenodithiophene and quinoxaline-based conjugated polymers for highly efficient polymer solar cells. Chem Mater 2011;23:2289–91. http://dx.doi.org/10.1021/cm200316s.

[9] Campos LM, Tontcheva A, Günes S, Sonmez G, Neugebauer H, Sariciftci NS, et al. Extended photocurrent spectrum of a low band gap polymer in a bulk heterojunction solar cell. Chem Mater 2005;17:4031–3. http://dx.doi.org/10.1021/cm050463+.

[10] Shi Q, Chen W-Q, Xiang J, Duan X-M, Zhan X. A low-bandgap conjugated polymer based on squaraine with strong two-photon absorption. Macromolecules 2011;44:3759–65. http://dx.doi.org/10.1021/ma200386f.

[11] Kang B, Lee SM. Nonlinear absorption properties of PPyPyV polymer. Opt Mater (Amst) 2010;32:1485–7. http://dx.doi.org/10.1016/j.optmat.2010.06.006.

[12] Bao Z, Lovinger AJ, Brown J. New air-stable n-channel organic thin film transistors. J Am Chem Soc 1998;120:207–8. http://dx.doi.org/10.1021/ja9727629.

[13] Zhou Y, Liu W-J, Ma Y, Wang H, Qi L, Cao Y, et al. Single microwire transistors of oligoarenes by direct solution process. J Am Chem Soc 2007;129:12386–7. http://dx.doi.org/10.1021/ja075045f.

[14] Wang H, Wen Y, Yang X, Wang Y, Zhou W, Zhang S, et al. Fused-ring pyrazine derivatives for n-type field-effect transistors. ACS Appl Mater Interfaces 2009;1:1122–9. http://dx.doi.org/10.1021/am900093p.

[15] Wöhrle D, Meissner D. Organic solar cells. Adv Mater 1991;3:129–38. http://dx.doi.org/10.1002/adma.19910030303.

[16] Zhou E, Cong J, Yamakawa S, Wei Q, Nakamura M, Tajima K, et al. Synthesis of thieno[3,4-b]pyrazine-based and 2,1,3-Benzothiadiazole-Based Donor–Acceptor copolymers and their application in photovoltaic devices. Macromolecules 2010;43:2873–9. http://dx.doi.org/10.1021/ma100039q.

[17] Abdo NI, Ku J, El-Shehawy AA, Shim H-S, Min J-K, El-Barbary AA, et al. Synthesis and characterization of low bandgap [small pi]-conjugated copolymers incorporating 4,7-bis(3,3[prime or minute]/4,4[prime or minute]-hexylthiophene-2-yl)benzo[c][2,1,3]thiadiazole units for photovoltaic application. J Mater Chem A 2013;1:10306–17. http://dx.doi.org/10.1039/C3TA11433C.

[18] Muller CD, Falcou A, Reckefuss N, Rojahn M, Wiederhirn V, Rudati P, et al. Multi-colour organic light-emitting displays by solution processing. Nature 2003;421:829–33.

[19] Du X, Qi J, Zhang Z, Ma D, Wang ZY. Efficient non-doped near infrared organic light-emitting devices based on fluorophores with aggregation-induced emission enhancement. Chem Mater 2012;24:2178–85. http://dx.doi.org/10.1021/cm3008733.

[20] Gu P-Y, Zhao Y, He J-H, Zhang J, Wang C, Xu Q-F, et al. Synthesis, physical properties, and light-emitting diode performance of phenazine-based derivatives with three, five, and nine fused six-membered rings. J Org Chem 2015. http://dx.doi.org/10.1021/jo5027707. 150309083752008.

[21] Chang DW, Lee HJ, Kim JH, Park SY, Park S-M, Dai L, et al. Novel quinoxaline-based organic sensitizers for dye-sensitized solar cells. Org Lett 2011;13:3880–3. http://dx.doi.org/10.1021/ol2012378.

[22] Eu S, Hayashi S, Umeyama T, Matano Y, Araki Y, Imahori H. Quinoxaline-fused porphyrins for dye-sensitized solar cells. J Phys Chem C 2008;112:4396–405. http://dx.doi.org/10.1021/jp710400p.

[23] Wu Y, Zhu W. Organic sensitizers from D-[small pi]-A to D-A-[small pi]-A: effect of the internal electron-withdrawing units on molecular absorption, energy levels and photovoltaic performances. Chem Soc Rev 2013;42:

2039–58. http://dx.doi.org/10.1039/C2CS35346F.

[24] Lu X, Feng Q, Lan T, Zhou G, Wang Z-S. Molecular engineering of quinoxaline-based organic sensitizers for highly efficient and stable dye-sensitized solar cells. Chem Mater 2012;24:3179–87. http://dx.doi.org/10.1021/cm301520z.

[25] Zhang L-P, Jiang K-J, Li G, Zhang Q-Q, Yang L-M. Pyrazino[2,3-g]quinoxaline dyes for solar cell applications. J Mater Chem A 2014;2:14852. http://dx.doi.org/10.1039/C4TA02499K.

[26] Bunz UHF. N-Heteroacenes. Chem – A Eur J 2009;15:6780–9. http://dx.doi.org/10.1002/chem.200900990.

[27] Bunz UHF, Engelhart JU, Lindner BD, Schaffroth M. Large N-Heteroacenes: new tricks for very old dogs? Angew Chem Int Ed 2013;52:3810–21. http://dx.doi.org/10.1002/anie.201209479.

[28] Gao B, Wang M, Cheng Y, Wang L, Jing X, Wang F. Pyrazine-containing acene-type molecular ribbons with up to 16 rectilinearly arranged fused aromatic rings. J Am Chem Soc 2008;130:8297–306. http://dx.doi.org/10.1021/ja800311a.

[29] Chen J, Cao Y. Development of novel conjugated donor polymers for high-efficiency bulk-heterojunction photovoltaic devices. Acc Chem Res 2009;42:1709–18. http://dx.doi.org/10.1021/ar900061z.

[30] Winkler M, Houk KN. Nitrogen-rich Oligoacenes: candidates for n-channel organic semiconductors. J Am Chem Soc 2007;129:1805–15. http://dx.doi.org/10.1021/ja067087u.

[31] Brownell LV, Robins KA, Jeong Y, Lee Y, Lee D- C. Highly Systematic and Efficient HOMO–LUMO Energy gap control of thiophene-pyrazine-acenes. J Phys Chem C 2013;117:25236–47. http://dx.doi.org/10.1021/jp407269p.

[32] Chen S, Raad FS, Ahmida M, Kaafarani BR, Eichhorn SH. Columnar mesomorphism of fluorescent board-shaped quinoxalinophenanthrophenazine derivatives with donor–acceptor structure. Org Lett 2013;15:558–61. http://dx.doi.org/10.1021/ol303375x.

[33] Xiao W, He Z, Remiro-Buenamañana S, Turner RJ, Xu M, Yang X, et al. A π-extended donor–acceptor–donor triphenylene twin linked via a pyrazine bridge. Org Lett 2015;17:3286–9. http://dx.doi.org/10.1021/acs.orglett.5b01444.

[34] Achelle S, Baudequin C, Plé N. Luminescent materials incorporating pyrazine or quinoxaline moieties. Dye Pigment 2013;98:575–600. http://dx.doi.org/10.1016/j.dyepig.2013.03.030.

[35] Estrada LA, Neckers DC. Synthesis and photophysics of dibenz- [a, c] phenazine derivatives. Org Lett 2011;13:3304. http://dx.doi.org/10.1021/jp-2011-00507j.3305.

[36] Zhang L, Lo KC, Chan WK. A new route to the synthesis of near-infrared absorbing pyrazinopyrazine bridged dyes with intramolecular charge transfer character. Chem Commun (Camb) 2014;50:4245–7. http://dx.doi.org/10.1039/c4cc01084a.

[37] Sıdır I, Sıdır YG. Ground state and excited state dipole moments of 6,8-diphenylimidazo[1,2-α]pyrazine determined from solvatochromic shifts of absorption and fluorescence spectra. Spectrochim Acta A Mol Biomol Spectrosc 2011;79:1220–5. http://dx.doi.org/10.1016/j.saa.2011.04.046.

[38] Lu X, Fan S, Wu J, Jia X, Wang ZS, Zhou G. Controlling the charge transfer in D-A-D chromophores based on pyrazine derivatives. J Org Chem 2014;79:6480–9. http://dx.doi.org/10.1021/jo500856k.

[39] Miller LL, Schlechte JS, Zinger B, Burrell CJ. Synthesis and electrochemistry of molecular dumbbells. Triblock copolymers of dendrons and rigid rods. Chem Mater 2002;14:5081–9. http://dx.doi.org/10.1021/cm0201908.

[40] Cheng Y-J, Wu J-S, Shih P-I, Chang C-Y, Jwo P-C, Kao W-S, et al. Carbazole-based ladder-type heptacylic arene with aliphatic side chains leading to enhanced efficiency of organic photovoltaics. Chem Mater 2011;23:2361–9. http://dx.doi.org/10.1021/cm200041v.

[41] Mitsopoulou CA, Veroni I, Philippopoulos AI, Falaras P. Synthesis, characterization and sensitization properties of two novel mono and bis carboxyl-dipyrido-phenazine ruthenium(II) charge transfer complexes. J Photochem Photobiol A Chem 2007;191:6–12. http://dx.doi.org/10.1016/j.jphotochem.2007.03.024.

[42] Geng J, Dai Y, Wang X-X, Hu M-Y, Tao T, Huang W. Substitution effects on the properties of 10,13-disubstituted dipyrido[3,2-a:2′,3′-c]phenazine donor–acceptor compounds and their ruthenium(II) complexes. Tetrahedron 2015;71:654–62. http://dx.doi.org/10.1016/j.tet.2014.12.017.

[43] Shigehiro T, Yagi S, Maeda T, Nakazumi H, Fujiwara H, Sakurai Y. Novel 10,13-disubstituted dipyrido[3,2-a:2′,3′-c]phenazines and their platinum(II) complexes: highly luminescent ICT-type fluorophores based on D–A–D structures. Tetrahedron Lett 2014;55:5195–8. http://dx.doi.org/10.1016/j.tetlet.2014.07.069.

[44] Bolligarla R, Das SK. Synthesis of new intramolecular charge transfer A–D–A tetrathiafulvalene-fused triads exhibiting large solvent sensitive emission behavior. Tetrahedron Lett 2011;52:2496–500. http://dx.doi.org/10.1016/j.tetlet.2011.03.016.

[45] Nietfeld JP, Schwiderski RL, Gonnella TP, Rasmussen SC. Structural effects on the electronic properties of extended fused-ring thieno[3,4-b]pyrazine analogues. J Org Chem 2011;76:6383–8. http://dx.doi.org/10.1021/jo200850w.

[46] Wang X, Zhou Y, Lei T, Hu N, Chen E-Q, Pei J. Structural–Property relationship in pyrazino[2,3-g]quinoxaline derivatives: morphology, photophysical, and waveguide properties. Chem Mater 2010;22:3735–45. http://dx.doi.org/10.1021/cm100798q.

[47] Bureš F, Čermáková H, Kulhánek J, Ludwig M, Kuznik W, Kityk IV, et al. Structure-property relationships and nonlinear optical effects in donor-substituted dicyanopyrazine-derived push-pull chromophores with enlarged and varied π-linkers. Eur J Org Chem 2012:529–38. http://dx.doi.org/10.1002/ejoc.201101226.

[48] Loving G, Imperiali B. A versatile amino acid analogue of the solvatochromic powerful tool for the study of dynamic protein interactions. J Am Chem Soc 2008;130:13630–8.

[49] Eugenio Vazquez M, Rothman DM, Imperiali B. A new environment-sensitive fluorescent amino acid for Fmoc-based solid phase peptide synthesis. Org Biomol Chem 2004;2:1965–6. http://dx.doi.org/10.1039/B408001G.

[50] Vázquez ME, Blanco JB, Imperiali B. Photophysics and Biological Applications of the environment-sensitive fluorophore 6-N,N-Dimethylamino-2,3-naphthalimide. J Am Chem Soc 2005;127:1300–6. http://dx.doi.org/10.1021/ja0449168.

[51] Nitz M, Mezo AR, Ali MH, Imperiali B. Enantioselective synthesis and application of the highly fluorescent and environment-sensitive amino acid 6-(2-dimethylaminonaphthoyl) alanine (DANA). Chem Commun 2002:1912–3. http://dx.doi.org/10.1039/B205224E.

[52] Tainaka K, Tanaka K, Ikeda S, Nishiza K, Unzai T, Fujiwara Y, et al. PRODAN-conjugated DNA: synthesis and photochemical properties. J Am Chem Soc 2007;129:4776–84. http://dx.doi.org/10.1021/ja069156a.

[53] Kim HM, Choo H-J, Jung S-Y, Ko Y-G, Park W-H, Jeon S-J, et al. A two-photon fluorescent probe for lipid raft imaging: C-Laurdan. ChemBioChem 2007;8:553–9. http://dx.doi.org/10.1002/cbic.200700003.

[54] Klymchenko AS, Pivovarenko VG, Ozturk T, Demchenko AP. Modulation of the solvent-dependent dual emission in 3-hydroxychromones by substituents. New J Chem 2003;27:1336–43. http://dx.doi.org/10.1039/B302965D.

[55] Schmitt V, Moschel S, Detert H. Diaryldistyrylpyrazines: solvatochromic and acidochromic fluorophores. Eur J Org Chem 2013;2013:5655–69. http://dx.doi.org/10.1002/ejoc.201300463.

[56] Takamuki Y, Maki S, Niwa H, Ikeda H, Hirano T. Substituent effects on the spectroscopic properties of solvatochromic 2-phenylimidazo[1,2-a]pyrazin-3(7H)-ones: an effective control for the colorimetric sensor properties. Tetrahedron 2005;61:10073–80. http://dx.doi.org/10.1016/j.tet.2005.08.008.

[57] Choudhary AS, Sekar N. Phenazine fused benzo coumarins with negative solvatochromism and positive solvatochromic emission - synthesis, photo physical properties, DFT and TDDFT studies. J Fluoresc 2015;25:675–84. http://dx.doi.org/10.1007/s10895-015-1553-x.

[58] Tathe AB, Sekar N. Novel fluorescent Phenazines: synthesis, characterization, photophysical properties and DFT calculations. J Fluoresc 2015;25:1403–15. http://dx.doi.org/10.1007/s10895-015-1631-0.

[59] Tolosa J, Solntsev KM, Tolbert LM, Bunz UHF. Unsymmetrical cruciforms. J Org Chem 2010;75:523–34. http://dx.doi.org/10.1021/jo901961a.

[60] Grabiec E, Kurcok M, Schab-Balcerzak E. Poly(amide imides) and poly(ether imides) containing 1,3,4-Oxadiazole or pyridine rings: characterizations and optical properties. J Phys Chem A 2009;113:1481–8. http://dx.doi.org/10.1021/jp807954w.

[61] Spitler EL, McClintock SP, Haley MM. Dynamic proton-induced emission switching in donor-functionalized Dehydrobenzopyrid[15]annulenes. J Org Chem 2007;72:6692–9. http://dx.doi.org/10.1021/jo070827c.

[62] Spitler EL, Shirtcliff LD, Haley MM. Systematic Structure–Property investigations and ion-sensing studies of pyridine-derivatized donor/acceptor tetrakis(arylethynyl)benzenes. J Org Chem 2007;72:86–96. http://dx.doi.org/10.1021/jo061712w.

[63] Achelle S, Nouira I, Pfaffinger B, Ramondenc Y, Plé N, Rodríguez-López J. V-Shaped 4,6-Bis(arylvinyl)pyrimidine oligomers: synthesis and optical properties. J Org Chem 2009;74:3711–7. http://dx.doi.org/10.1021/jo900107u.

[64] Benassi E, Carlotti B, Fortuna CG, Barone V, Elisei F, Spalletti A. Acid–Base strength and acidochromism of some dimethylamino–azinium iodides. An integrated experimental and theoretical study. J Phys Chem A 2015;119:323–33. http://dx.doi.org/10.1021/jp510982h.

[65] Li G, Abiyasa AP, Gao J, Divayana Y, Chen W, Zhao Y, et al. Synthesis and properties of a diazopentacene analogue. Asian J Org Chem 2012;1:346–51. http://dx.doi.org/10.1002/ajoc.201200120.

[66] Singh P, Baheti A, Thomas KRJ. Synthesis and optical properties of acidochromic amine-substituted benzo[a]phenazines. J Org Chem 2011;76:6134–45. http://dx.doi.org/10.1021/jo200857p.

[67] Publication A. 1,2-Naphthoquinone-4-Sulfonate, ammonium and potassium. Org Synth 1941;21:91. http://dx.doi.org/10.15227/orgsyn.021.0091.

[68] Zhang H, Fan J, Wang J, Dou B, Zhou F, Cao J, et al. Fluorescence discrimination of Cancer from inflammation by molecular response to COX-2 enzymes. J Am Chem Soc 2013;135:17469–75. http://dx.doi.org/10.1021/ja4085308.

[69] Kim H-J, Lee E, Park H, Lee M. Dynamic Extension–Contraction motion in supramolecular springs. J Am Chem Soc 2007;129:10994–5. http://dx.doi.org/10.1021/ja073554b.

[70] Kohn W, Sham LJ. Self-consistent equations including exchange and correlation effects. Phys Rev 1965;140:A1133–8. http://dx.doi.org/10.1103/PhysRev.140.A1133.

[71] Becke AD. A new mixing of Hartree–Fock and local density-functional theories. J Chem Phys 1993;98:1372. http://dx.doi.org/10.1063/1.464304.

[72] Lee C, Yang W, Parr RG. Development of the Colle-Salvetti correlation-energy formula into a functional of the electron density. Phys Rev B 1988;37:785–9. http://dx.doi.org/10.1103/PhysRevB.37.785.

[73] Scalmani G, Frisch MJ, Mennucci B, Tomasi J, Cammi R, Barone V. Geometries and properties of excited states in the gas phase and in solution: theory and application of a time-dependent density functional theory polarizable continuum model. J Chem Phys 2006;124:94107. http://dx.doi.org/10.1063/

1.2173258.

[74] Tomasi J, Mennucci B, Cammi R. Quantum mechanical continuum solvation models. Chem Rev 2005;105:2999–3094. http://dx.doi.org/10.1021/cr9904009.

[75] Van Gemert B, Knowles DB. Photochromic naphthopyran compounds. 1996. US5552090A.

[76] Rickwood M, Marsden SD, Askew VE. Photochromic spiroxazine compounds. 1995. US5446150 A.

[77] Clarke DA, Heron BM, Gabbutt CD, Hepworth JD, Partington SM, Corns SN. Photochromic compounds. 1999. WO1999020630 A1.

[78] Bodige S, MacDonnell FM. Synthesis of free and ruthenium coordinated 5,6-diamino-1,10-phenanthroline. Tetrahedron Lett 1997;38:8159–60. http://dx.doi.org/10.1016/S0040-4039(97)10223-4.

[79] Lippert E. Spektroskopische Bestimmung des Dipolmomentes aromatischer Verbindungen im ersten angeregten Singulettzustand. Zeitschrift Für Elektrochemie. Berichte Der Bunsenges Für Phys Chem 1957;61:962–75. http://dx.doi.org/10.1002/bbpc.19570610819.

[80] McRae EG. Theory of solvent effects on molecular electronic spectra. Frequency shifts. J Phys Chem 1954;61:1957. http://dx.doi.org/10.1021/j150551a012.

[81] Ravi M, Samanta A, Radhakrishnan TP. Excited state dipole moments from an efficient analysis of solvatochromic stokes shift data. J Phys Chem 1994;98: 9133–6. http://dx.doi.org/10.1021/j100088a007.

[82] Reichardt C. Solvatochromic dyes as solvent polarity indicators. Chem Rev 1994;94:2319–58. http://dx.doi.org/10.1021/cr00032a005.

[83] Kamlet MJ, Taft RW. The solvatochromic comparison method. I. The.beta.-scale of solvent hydrogen-bond acceptor (HBA) basicities. J Am Chem Soc 1976;98:377–83. http://dx.doi.org/10.1021/ja00418a009.

[84] Kamlet MJ, Abboud JL, Taft RW. The solvatochromic comparison method. 6. The.pi.* scale of solvent polarities. J Am Chem Soc 1977;99:6027–38. http://dx.doi.org/10.1021/ja00460a031.

[85] Catalán J, López V, Pérez P, Martin-Villamil R, Rodríguez J-G. Progress towards a generalized solvent polarity scale: the solvatochromism of 2-(dimethylamino)-7-nitrofluorene and its homomorph 2-fluoro-7-nitrofluorene. Liebigs Ann 1995;1995:241–52. http://dx.doi.org/10.1002/jlac.199519950234.

[86] Catalán J, Díaz C. Extending the solvent acidiy scale to highly acidic organic solvents: the unique photophysical behaviour of 3,6-Diethyltetrazine. Eur J Org Chem 1999;1999:885–91. http://dx.doi.org/10.1002/(SICI)1099-0690(199904)1999. 4<885::AID-EJOC885>3.0.CO;2-W.

[87] Catalán J, Hopf H. Empirical treatment of the inductive and dispersive components of Solute–Solvent interactions: the solvent polarizability (SP) scale. Eur J Org Chem 2004;2004:4694–702. http://dx.doi.org/10.1002/ejoc.200400311.

[88] Hofmann K, Schreiter K, Seifert A, Ruffer T, Lang H, Spange S. Solvatochromism and linear solvation energy relationship of diol- and proline-functionalized azo dyes using the Kamlet-Taft and Catalan solvent parameter sets. New J Chem 2008;32:2180–8. http://dx.doi.org/10.1039/B809055F.

[89] Catalán J. Toward a generalized treatment of the solvent effect based on four empirical scales: dipolarity (SdP, a new scale), polarizability (SP), acidity (SA), and basicity (SB) of the medium. J Phys Chem B 2009;113:5951–60. http://dx.doi.org/10.1021/jp8095727.

[90] Gaussian 09 Citation n.d. http://www.gaussian.com/g_tech/g_ur/m_citation.htm (accessed December 18, 2015).